Journal of Catalysis **194,** 175–187 (2000)
doi:10.1006/jcat.2000.2942, available online at http://www.idealibrary.com on IDEAL®

Reaction and Deactivation Pathways in Xylene Isomerization on Zirconia Modified by Tungsten Oxide

Ryan D. Wilson,[1] David G. Barton,[2] Chelsey D. Baertsch, and Enrique Iglesia[3]

Department of Chemical Engineering, University of California at Berkeley, Berkeley, California 94720

Received October 27, 1999; revised May 30, 2000; accepted May 31, 2000

The effect of H_2 on isomerization pathways and on the acid site density on WO_x-ZrO_2 catalysts was explored using kinetic measurements of acid-catalyzed *o*-xylene isomerization reactions. Initial *o*-xylene isomerization rates on WO_x-ZrO_2 at 523 K are proportional to the H_2 concentration even though H atoms are not involved directly in reaction turnovers, as shown by the low deuterium content in the isomers formed from D_2/*o*–C_8H_{10} mixtures. H_2 chemisorption uptakes on WO_x-ZrO_2 and isomerization rates show a similar dependence on WO_x surface density and structure, suggesting that Brønsted acid sites form via reductive processes that require H atoms from H_2. This proposal is consistent with UV-visible spectra, which show the formation of reduced centers by H_2; these centers correspond to the formation of acidic $H^{\delta+}$ species with charge compensation by $WO_3^{\delta-}$ domains. The transients induced by the addition and removal of H_2 (or O_2) during xylene isomerization show that the formation of acid sites by H_2 is reversible at reaction conditions and that H_2 is involved in maintaining a steady-state density of acid sites. H_2 also inhibits catalyst deactivation, apparently by reversing C–H bond activation steps leading to the formation of strongly adsorbed unsaturated hydrocarbons. A sequence of elementary steps including isomerization, deactivation, and acid site formation pathways was found to describe accurately the observed effects of H_2 and *o*-xylene on deactivation, reaction rates, and the results of *o*-$^{13}C_8H_{10}$/*o*-C_8H_{10} and D_2/*o*-C_8H_{10} exchange experiments.

Key Words: **xylene isomerization; tungsten oxide; deactivation pathways; Brønsted acid.**

INTRODUCTION

Recent studies have addressed the synthesis of WO_x-ZrO_2 acid catalysts (1) and their use in acid-catalyzed isomerization reactions (2–5) after treatment at high temperatures, which lead to the formation of two-dimensional polytungstate domains. The treatment temperature required for maximum rates increases with decreasing W concentration, and *o*-xylene isomerization rates depend only on the WO_x surface density (reaching a maximum at $\sim$10 WO_x/nm^2) rather than the W concentration or treatment temperature independently (6, 7).

H_2 and the presence of Pt clusters on WO_x-ZrO_2 led to stable high rates and selectivity for *n*-heptane isomerization (8). In this case, H_2 is used in hydrogen transfer steps required for desorption of adsorbed isomers. Xylene isomerization pathways are also influenced by H_2 on metal-free WO_x-ZrO_2 (6), even though H_2 is not involved in the reaction stoichiometry, metal sites are not available to dissociate H_2, and hydrogen transfer steps are not required for *o*-xylene isomerization turnovers, which involve protonation–deprotonation steps with interspersed methyl shifts. The promoting effect of H_2 on xylene isomerization rates is complicated by the concurrent effect of H_2 on deactivation rates, which requires that rates be extrapolated to early times on stream.

This study explores reaction and deactivation pathways for *o*-xylene isomerization on WO_x-ZrO_2 catalysts and the role of H_2 in catalytic turnovers and less frequent side events that form irreversibly adsorbed species and lead to deactivation. The effect of xylene and H_2 concentrations on *initial* isomerization rates and the isotopic exchange between *o*-C_8H_{10}/D_2 and *o*-$^{13}C_8H_{10}$/*o*-C_8H_{10} mixtures were used to explore elementary step sequences required for isomerization turnovers for the formation and destruction of active sites via hydrogen desorption or formation–desorption of unsaturated carbonaceous deposits.

EXPERIMENTAL

Catalyst Synthesis

High surface area $ZrO_x(OH)_{4-2x}$ was prepared by precipitation of a zirconyl chloride ($ZrOCl_2 \cdot 8H_2O$, Aldrich, >98%, Hf <0.5%; 0.5 M) solution with NH_4OH (14 N) at a constant pH of 10. The precipitate was filtered and slurried in deionized water until the addition of $AgNO_3$ to the filtrate did not detect the presence of Cl^- ions. The $ZrO_x(OH)_{4-2x}$ gel was dried at 383 K overnight, crushed, and sieved to retain 0.12–0.38 mm particles. The dried

[1] Current address: UCR College of Engineering Center for Environmental Research and Technology (CE-CERT), Riverside, CA 92507.
[2] Current address: Dow Chemical Company, Midland, MI 48674.
[3] To whom correspondence should be addressed. E-mail: iglesia@cchem.berkeley.edu.

0021-9517/00 $35.00

particles were impregnated to the point of incipient wetness with a solution of ammonium metatungstate ($(NH_4)_6H_2W_{12}O_{40}$, Strem Chemicals, 99.9%) to give 15 wt% WO_3 or 30 wt% WO_3 after calcination. These samples were dried in air at 383 K overnight and then treated in flowing air (Linde Zero Grade, 3.3 $cm^3\ s^{-1}$, purified using Drierite and 13X molecular sieve traps) by heating to 1073 K (for 15 wt% WO_3) or 973 K (for 30 wt% WO_3) at 0.167 $K\,s^{-1}$ and holding for 3 h. These treatments led to WO_3 surface densities of 11.7 WO_x/nm^2 and 8.4 WO_x/nm^2; maximum *o*-xylene isomerization rates are observed for samples within this range of surface densities (7). H-ZSM5 was prepared by exchanging Na–ZSM5 (Zeochem, Si/Al = 14.5) with a solution of 0.16 M NH_4NO_3 at 353 K for 16 h in order to form NH_4–ZSM5 and then treating the latter in dry air at 773 K for 20 h to form H-ZSM5.

Catalyst Pretreatment

WO_x-ZrO_2 samples were treated in dry air at 823 K for 1 h and cooled to 423 K in air before catalytic measurements. The samples were then flushed with He, heated to 523 K in flowing H_2 for 1 h and exposed to the reactant mixture at 523 K. This treatment was also used in order to restore initial *o*-xylene isomerization rates on deactivated WO_x-ZrO_2 catalysts.

o-Xylene Reaction Studies

o-Xylene isomerization was carried out at 523 K in a flow reactor with plug-flow hydrodynamics. The reactants were introduced by flowing a carrier gas (He, H_2, or H_2/He mixtures) through a thermostated saturator containing liquid *o*-xylene (Reidel De Haen, >99%). H_2 (Praxair, UHP) was purified using a Pd/Al_2O_3 catalyst and a 13X sieve in order to remove O_2 and H_2O, respectively. He (Praxair, UHP) was purified using a 13X sieve and an oxygen absorber (Matheson). *o*-Xylene was used without further purification. *o*-Xylene concentrations were measured by gas chromatography (Hewlett–Packard 5890 GC) using flame ionization detection and inert CH_4 as an internal standard. Xylene isomers were separated using a DB-WAX capillary column (J&W Scientific).

Isotopic Tracer Studies

The role of H_2 in *o*-xylene isomerization turnovers was examined by measuring isotopic exchange rates in mixtures of D_2 (Matheson, 99.5%) and *o*-C_8H_{10} (523 K, 145 kPa D_2, 0.66 kPa *o*-xylene) on WO_x-ZrO_2. The deuterium content in reactants and products was measured by mass spectrometry using previously reported procedures (9) and a 5890 Hewlett–Packard gas chromatograph equipped with a mass selective detector. The mechanism of *o*-xylene isomerization was studied by measuring the rate of exchange between equimolar mixtures of doubly ^{13}C-labeled (at methyl groups) and unlabeled *o*-xylene reactants. Xylenes were labeled with ^{13}C in both methyl positions and singly labeled isotopomers were used as a diagnostic of intermolecular methyl shifts typical of bimolecular pathways. These isotopic exchange reactions were conducted in a glass recirculating batch reactor at 523 K and a total pressure of 107 kPa (0.67 kPa *o*-xylene, 106 kPa H_2 or He, 0.030 g sample). This reactor has a total volume of 690 cm^3, a gas recirculation rate of 4.2 $cm^3\ s^{-1}$, and it is operated at less than 2% reactant conversion per pass in order to ensure gradientless operation (10). The reactor can be evacuated using mechanical and diffusion pumps isolated from the system by liquid N_2 traps. *o*-Xylene (NBS, >99.995%), was purified by multiple freeze–evacuation–thaw cycles and it was introduced as a vapor from liquid held at room temperature.

Data Analysis Procedures

Reaction rates are reported as the number of molecules of *o*-xylene reacted per W-atom in the catalyst sample per second. These rates become turnover rates if all WO_x species are active and accessible to reactants. Product selectivities are reported on a carbon basis, as the percentage of the *o*-xylene molecules converted that appears as isomerization products (*p*-xylene, *m*-xylene) or disproportionation products (toluene, trimethyl-benzene isomers). Xylene hydrogenation products were not detected even at the highest temperatures (623 K) and H_2 pressures (124 kPa) of this study. The space velocity in flow reactor experiments is defined as the mass of hydrocarbons contacting a given catalyst mass per hour. The observed deactivation required that rates be extrapolated to zero time in order to determine initial reaction rates. The initial reaction rate was determined by linear extrapolation of a semi-logarithmic plot of the reaction rate versus time on stream. Catalytic data were collected at low conversions (<5%); at these conditions, the concentration of reactants varies only slightly with catalyst deactivation. This allows measurements of deactivation rates at initial values of reactant concentrations. A linear regression analysis was used to calculate 95% confidence limits for *o*-xylene isomerization kinetic parameters (rate constants, equilibrium constants, activation energies, etc.) (see (11) for details).

RESULTS AND DISCUSSION

o-Xylene Isomerization Rates and Selectivity

o-Xylene isomerization proceeds via sequential intramolecular or intermolecular methyl shifts to form *m*-xylene and *p*-xylene (12); the unimolecular isomerization pathways involve only protonation–deprotonation pathways with interspersed methyl shifts before desorption

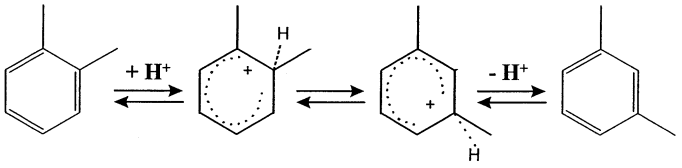

SCHEME 1. Protonation/deprotonation steps and intramolecular methyl shifts in *o*-xylene isomerization (12).

(Scheme 1). The equilibrium ortho : meta : para-xylene ratio at 523 K is 1 : 2.5 : 1.1 (13).

o-Xylene isomerization rates and selectivities in He and H_2 are shown in Table 1 at similar *o*-xylene conversions (3.6–4.2%) for WO_x-ZrO_2. The slight difference in conversion levels in Table 1 cannot account for the selectivity differences caused by H_2, because selectivity depends weakly on conversion (Fig. 1). Toluene and trimethylbenzene isomers were formed in approximately equimolar amounts via intermolecular methyl shifts.

m-Xylene is the initial product of a methyl shift in adsorbed *o*-xylene. The low para/meta-xylene isomer ratios shown in Table 1 suggest that adsorbed intermediates often desorb before a second methyl shift occurs. This is also apparent from the para/meta-xylene isomer ratio which approaches zero at low conversions (Fig. 2). This is consistent with rapid (quasi-equilibrated) adsorption–desorption of all xylene isomers, by which desorption occurs before multiple methyl shifts.

Initial isomerization rates on WO_x-ZrO_2 (per W atom) and H-ZSM5 (per Al) (shown in Table 1) are comparable between the two catalysts when H_2 is added to WO_x-ZrO_2. The presence of H_2 has no effect on *o*-xylene isomerization rates on H-ZSM5. When initial isomerization rates are normalized by the number of H atoms in WO_x-ZrO_2 (from H_2 chemisorption uptakes) and H-ZSM5 (from Al content), WO_x-ZrO_2 shows much higher isomerization turnover rates (Table 1). The H-atom concentration used in this calculation was determined from H_2 chemisorption uptakes at 523 K and 80 kPa H_2 (14). These data show that turnover rates (per site titrated by H atoms) are about 15 times higher on WO_x-ZrO_2 than on H-ZSM5.

H-ZSM5 exhibits a higher selectivity to isomerization products because the formation of bimolecular trans-alkylation transition states is restricted by H-ZSM5 channels (15). In addition, para/meta-xylene isomer ratios higher

TABLE 1

Results of *o*-Xylene Isomerization Reaction over 15 wt% WO_x-ZrO_2. (1073 K Oxidation, 8.4 $WO_x\,nm^{-2}$) and H-ZSM5 (Si/Al = 14.5)

	WO_x-ZrO_2		H-ZSM5 (Si/Al = 14.5)	
Hydrogen pressure (kPa)	0	124	0	125
o-Xylene conversion (%)	3.6	4.2	6.2	4.9
Initial isomerization turnover rate (10^{-3} s^{-1} per W or Al atom)*	0.2	1.7	1.8	1.8
Specific isomerization rate (h^{-1})**	5.4	44.5	81.8	82.3
Initial isomerization turnover rate (10^{-3} s^{-1} per H atom)***	—	26.0	1.8	1.8
Weight hourly space velocity (*g*-xylene/*g*-cat*h)	1.5	10.6	13.2	16.8
Isomerization selectivity (%)	90.8	96.7	99.7	99.8
Disproportionation selectivity (%)	9.2	3.3	0.3	0.2
Para/meta-xylene ratio (10^{-2})	4.4	4.7	83.3	66.7
Toluene/trimethylbenzenes ratio	1.3	0.9	1.5	1.6

Note. 523 K, 0–124 kPa H_2, 0.66 kPa *o*-xylene.

* Per W-atom on WO_x-ZrO_2; per Al-atom on H-ZSM5.

** Mass of *o*-xylene reacted per mass of catalyst sample.

*** Per chemisorbed H-atom on WO_x-ZrO_2 (14) and per Al atom H-ZSM5.

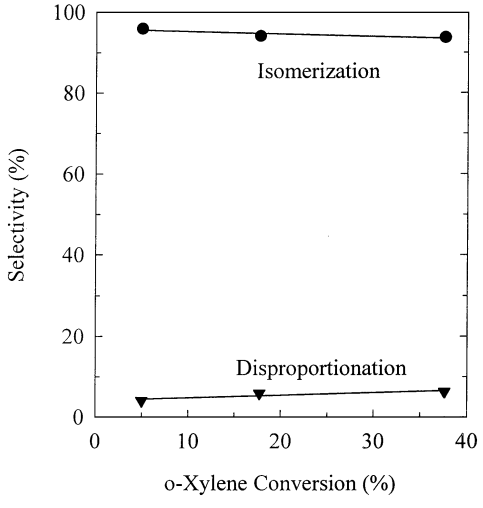

FIG. 1. Effect of conversion on selectivity to isomerization and disproportionation products (523 K, 124 kPa H_2, 0.66 kPa *o*-xylene, 15 wt% WO_x-ZrO_2; 8.4 WO_x/nm^2 surface density).

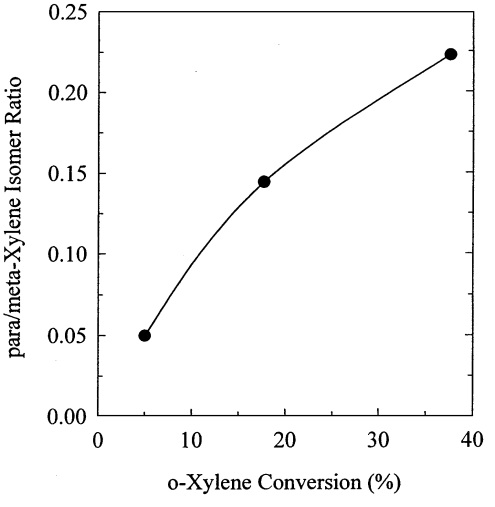

FIG. 2. Para/meta-Xylene isomer ratio as a function of residence time (523 K, 124 kPa H_2, 0.66 kPa *o*-xylene, 15 wt% WO_x-ZrO_2; 8.4 WO_x/nm^2 surface density).

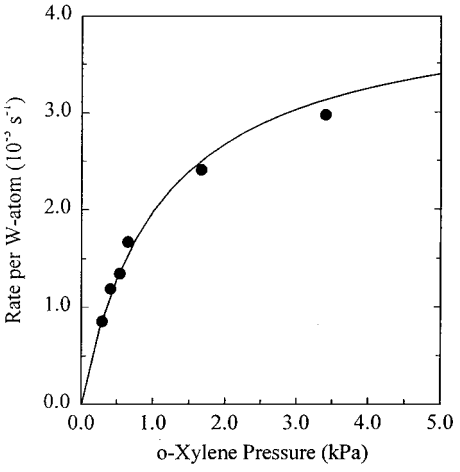

FIG. 3. Kinetic dependence on *o*-xylene concentration. Solid line represents the predicted dependence based on the values of the kinetic parameters predicted from Eq. [1] (523 K, 124 kPa H_2, 0.2–3.5 kPa *o*-xylene, 15 wt% WO_x-ZrO_2; 8.4 WO_x/nm^2 surface density).

than equilibrium values are observed on H-ZSM5, because para-xylene diffuses through ZSM-5 channels much faster than meta-xylene.

The Effect of o-Xylene Concentration on Isomerization Rates

The kinetic dependence of isomerization reaction rates on *o*-xylene pressure was measured by varying *o*-xylene pressures between 0.23 kPa and 5.12 kPa at reaction temperatures of 523, (Fig. 3), 573, and 623 K, and a constant H_2 pressure of 124 kPa. Initial isomerization rates increased with increasing *o*-xylene pressure and approached a constant value as *o*-xylene concentrations increased. These data are consistent with Langmuir–Hinshelwood kinetics on a surface that approaches *o*-xylene saturation coverage with increasing reactant concentration. *o*-Xylene reaction orders range from a value of one at low pressures (<1 kPa) to a value of zero at high pressures (>5 kPa). These data suggest that the surface is relatively free of adsorbed xylene at the conditions leading to the sharp maximum in xylene rates observed at intermediate WO_x surface densities (0.66 kPa *o*-xylene).

Elementary Steps in o-Xylene Isomerization on WO_x-ZrO_2

The dependence of isomerization rates on *o*-xylene concentration is consistent with a monomolecular mechanism, in which xylenes interact with single active sites via quasi-equilibrated adsorption–desorption followed by irreversible intramolecular methyl shifts (Scheme 2).

In Scheme 2, * represents an active site (H^+, Brønsted acid site) and X and X′ represent *o*-xylene and other xylene isomers, respectively. The first-order dependence on *o*-xylene at low concentrations (Fig. 3) is consistent with

1)	X + *	⇄	X*	K_1
2)	X*	→	X'*	k_2
3)	X'*	⇄	X' + *	K_3

SCHEME 2. Elementary steps in steady state *o*-xylene isomerization.

monomolecular isomerization pathways because bimolecular pathways would lead to a second-order dependence at sufficiently low concentrations.

The monomolecular nature of the isomerization reaction was verified by reactions of an equimolar *o*-$^{13}C_8H_{10}$/*o*-C_8H_{10} mixture at 523 K and 0.66 kPa total *o*-xylene pressure. Bimolecular isomerization requires a trans-alkylation step to form toluene and trimethylbenzene, followed by another intermolecular methyl shift between trimethylbenzene and xylene or toluene to form all possible xylene isomers (16). Bimolecular isomerization of a 50/50 mixture of doubly labeled (^{13}C at methyl groups) and unlabeled *o*-xylene would lead to the formation of singly labeled, doubly labeled, and unlabeled xylene isomers, with the singly labeled isomers accounting for approximately 50% of the total, but monomolecular isomerization would only lead to unlabeled and doubly labeled isomers (Scheme 3). Figure 4 shows the abundance of xylenes containing a single ^{13}C atom as a function of *o*-xylene conversion, which was collected in a recirculating batch reactor. The fraction of singly labeled ^{13}C atoms in all xylene isomers is never larger than 0.03, indicating that bimolecular reactions constitute a maximum of ~6% of the total rate. The percentage of *m*- and *p*-xylenes containing a single ^{13}C isotopic label decreases with increasing contact time (increasing conversion) because of dilution by unlabeled and doubly ^{13}C labeled *m*- and *p*-xylenes. This decrease could also be due in part to the rapid deactivation of sites that initially catalyzed minority bimolecular

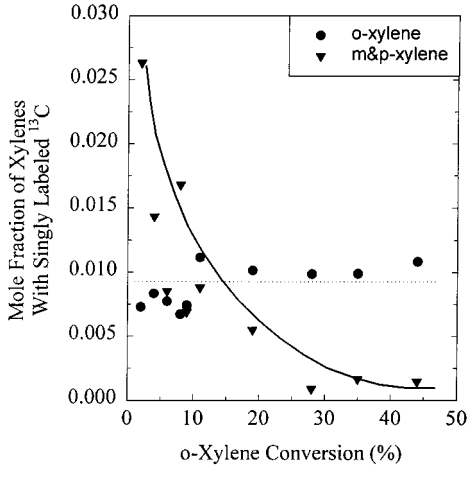

FIG. 4. Mole fraction of xylenes formed via a bimolecular mechanism (i.e., containing a single ^{13}C isotopic label) as a function of *o*-xylene conversion (523 K, 114 kPa H_2, 0.66 kPa *o*-xylene, 15 wt% WO_x-ZrO_2; 8.4 WO_x/nm^2 surface density).

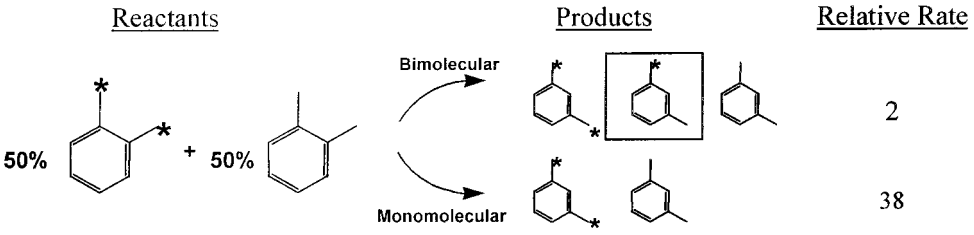

SCHEME 3. Expected products of reactions with doubly ^{13}C labeled and unlabeled xylene mixtures via bimolecular and monomolecular pathways (* represents a ^{13}C isotopic label). For simplicity only *m*-xylene products are shown (523 K, 112 kPa H_2, 0.66 kPa *o*-xylene).

pathways, which would be in agreement with previous batch reactor data that showed a high initial selectivity (~10%) to disproportionation products, which are also formed via bimolecular pathways (6, 7). The ratio of monomolecular to bimolecular isomerization rates (obtained from the concentration of singly labeled ^{13}C xylenes in products) is about 20, indicating that the contribution to isomerization products from bimolecular pathways is negligible on WO_x-ZrO_2.

The para/meta-xylene isomer ratios in Table 1 (~0.05) are much lower than the equilibrium ratios (0.44), suggesting that steps involving methyl shifts are not quasi-equilibrated during *o*-xylene isomerization on WO_x-ZrO_2. The rate expression (Eq. [1]) obtained with the assumption of quasi-equilibrated adsorption–desorption steps (an assumption confirmed later by D_2/*o*-xylene exchange reactions) and of irreversible intramolecular methyl shift steps (see Scheme 2) is consistent with experimental rate data:

$$r_i = \frac{k_2 K_1 (X)(L)}{1 + K_1 (X)}. \qquad [1]$$

In this expression, we have neglected a term corresponding to the adsorption of xylene isomer products in the denominator ($K_3(X')$), because at the low conversions of our experiments (<5%) the predominant xylene isomer is *o*-xylene and adsorption equilibrium constants for *o*-xylene (K_1) and *m*- and *p*-xylene (K_3) should be very similar. The kinetic parameters k_2 and K_1 (in Eq. [1]) shown in Fig. 5 were obtained from plots of the inverse reaction rate versus *o*-xylene pressure at several temperatures using linear least-squares methods. The predicted dependencies of isomerization rates on *o*-xylene concentration, using the calculated values of k_2 and K_1, are in excellent agreement with the experimental data (Fig. 6).

Apparent activation energies and preexponential factors for methyl shifts and enthalpy and entropy values for xylene adsorption on WO_x-ZrO_2 were determined from Arrhenius and van't-Hoff plots of k_2 and K_1, respectively (Table 2). Transition state theory predicts preexponential factors of $\sim 10^{13}\ s^{-1}$ (~kT/h) for monomolecular isomerization reactions, because the structure and properties of activated complexes resemble those of the adsorbed reactants. The measured preexponential factor (8.5×10^6) is about 10^6 times smaller than predicted from transition state theory. This discrepancy appears to reflect a mechanistic role of H_2 on the density of acid sites and on reaction rates (Table 1), which is not included in the kinetic steps of Scheme 2. Thus, kinetic parameters describing the effect of H_2 on the density of acid sites have been lumped into the measured value of k_2 (Eq. [1]). The apparent activation energy required for the methyl shift step is comparable to that measured on H–Y (17), suggesting that similar isomerization pathways requiring Brønsted acids are involved in H–Y and WO_x-ZrO_2 catalysts.

The measured enthalpy (−16.6 kcal/mol) and entropy (−31.7 cal/mol K) for xylene adsorption suggest that adsorbed xylene is mobile on WO_x-ZrO_2 materials. The adsorption entropy agrees well with that calculated (18) for the loss of a single degree of freedom during adsorption (−30.9 cal/mol K). The relatively low enthalpy of adsorption suggests that surface diffusion should occur at rates comparable to turnover rates at typical reaction temperatures (523 K).

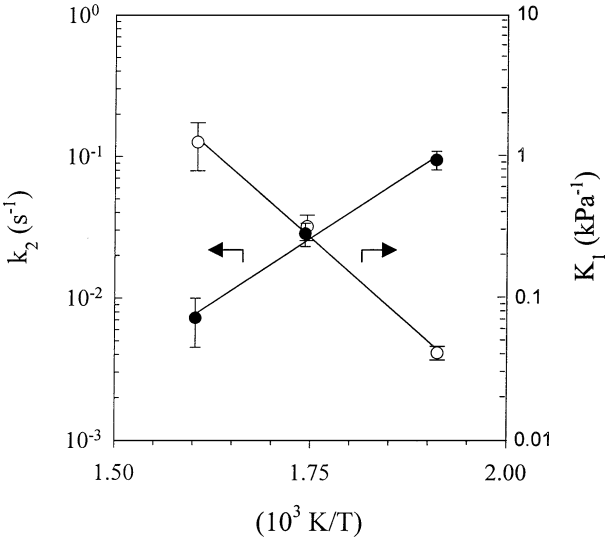

FIG. 5. Rate constants and adsorption/desorption equilibrium constants for *o*-xylene isomerization over 15% WO_x-ZrO_2 as a function of reaction temperature. Error bars represent 95% confidence limits and straight lines constitute a linear least-squares fit of the data (523–623 K, 124 kPa H_2, 0.66 kPa *o*-xylene, 15 wt% WO_x-ZrO_2; 8.4 WO_x/nm^2 surface density).

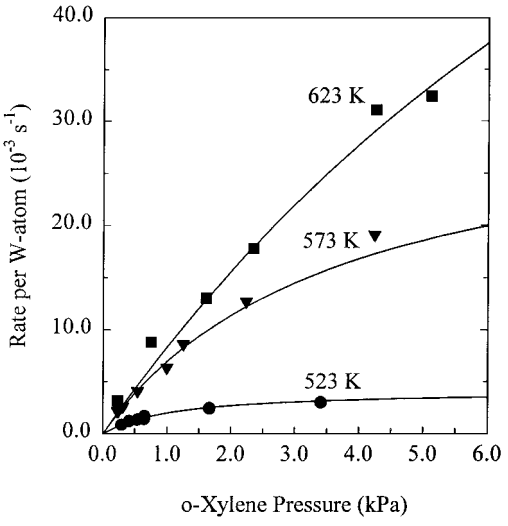

FIG. 6. *o*-Xylene isomerization rates as a function of reaction temperature and *o*-xylene pressure. Solid lines show the predicted dependence based on the values of k_2 and K_1 shown in Fig. 3 (523 K, 124 kPa H_2, 0.24–5.2 kPa *o*-xylene, 15 wt% WO_x-ZrO_2; 8.4 WO_x/nm^2 surface density).

The Effect of WO_x Surface Density on o-Xylene Isomerization Kinetics

The effect of WO_x surface density on the active site concentration and the acid strength was examined by measuring *o*-xylene isomerization kinetics. Since *o*-xylene isomerization rates depend only on WO_x surface density, rather than W loading or treatment temperature independently (6, 7), a 30 wt% WO_x-ZrO_2 sample treated in air at 988 K (11.7 WO_x/nm^2) was compared to a 15 wt% WO_x-ZrO_2 sample treated in air at 1073 K (8.4 WO_x/nm^2). These two catalysts have different activities due to differences in surface density and thus structure. Table 3 shows the values of the rate constant for the methyl shift step (k_2) and for the xylene adsorption/desorption equilibrium constant (K_1) on these two catalysts, as well as the initial turnover rate. The value of K_1 for the 11.7 WO_x/nm^2 sample is slightly lower than for the 8.4 WO_x/nm^2 sample, suggesting that the acid strength on the former is slightly lower than on the latter, since adsorption equilibrium constants reflect the stability

TABLE 2

Preexponential Factors, Activation Energies, Heat of Adsorption, and Entropy Change of Adsorption for *o*-Xylene Isomerization on 15 wt% WO_x-ZrO_2 and H-USY

	WO_x/ZrO_2	H-USY* [17] Si/Al = 3
A, s^{-1}	$8.5 \pm 1.0 \times 10^6$	8.6×10^{11}
E_a, kcal/mol	22.2 ± 2.7	29.0
ΔH_{ads}, kcal/mol	-16.6 ± 2.1	−20.20
ΔS_{ads}, cal/mol K	-31.7 ± 4.2	—

Note. Values are given for the reaction *o*-xylene → *m*-xylene.

TABLE 3

Methyl Shift Rate Constants (k_2) and Xylene Adsorption/Desorption Constants (K_1) for 15 wt% WO_x-ZrO_2 (8.4 WO_x/nm^2) and 30 wt% WO_x-ZrO_2 (11.7 WO_x/nm^2)

WO_x surface density	15 wt% WO_x-ZrO_2 8.4 WO_x/nm^2	30 wt% WO_x-ZrO_2 11.7 WO_x/nm^2
k_2, 10^{-3} s^{-1}	4.1 ± 0.6	11.2 ± 2.4
K_1, kPa^{-1}	0.9 ± 0.1	0.6 ± 0.1
Rate, 10^{-3} s^{-1}	1.5	3.2

Note. 523 K, 124 kPa H_2, 0.66 kPa, *o*-xylene.

of protonated xylenes and thus increases with increasing acid strength. The methyl shift rate constant (k_2) is almost 3 times larger on the 11.7 WO_x/nm^2 sample, which also has the higher initial rate (Table 3). Differences in rates are clearly due to changes in k_2, rather than K_1, indicating that significant changes in WO_x-ZrO_2 activity with varying WO_x surface density are not due to changes in acid strength.

The Effect of H_2 Concentration on o-Xylene Isomerization Rates

The effect of H_2 on initial isomerization rates was measured by varying the H_2 pressure between 0 and 124 kPa at 0.66 kPa *o*-xylene and 523 K (Fig. 7). The catalyst was treated in H_2 at the reaction temperature and H_2 pressure for 1 h before catalytic experiments in order to avoid transient effects after initial introduction of H_2/xylene reactants. Isomerization rates increased linearly with increasing H_2 concentration (Fig. 7). These data were obtained at conditions (0.66 kPa *o*-xylene) leading to catalyst surfaces relatively free of adsorbed xylene (i.e., $K(X) \ll 1$). Thus, the observed increase in turnover rates with increasing H_2

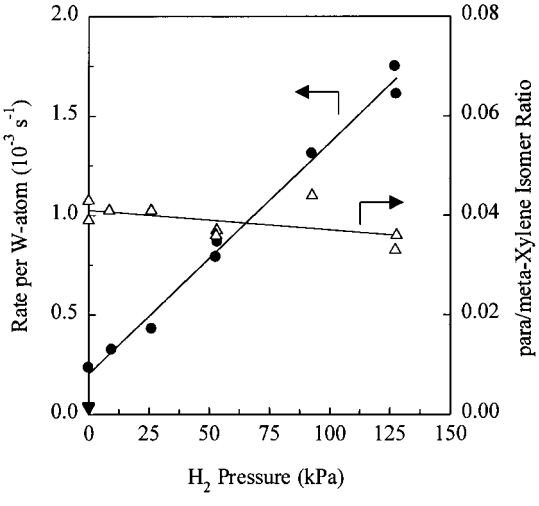

FIG. 7. Reaction rate and product xylene distribution dependence on H_2 pressure. Para/meta-Xylene isomer ratios measured at 4.0% (±0.5%) conversion (523 K, 0–124 kPa H_2, 0.66 kPa *o*-xylene, 15 wt% WO_x-ZrO_2; 8.4 WO_x/nm^2 surface density).

suggests that the rate expression must contain a H_2 dependence that has been inadvertently lumped into the value of k_2 reported in the previous section.

Isomerization rates are proportional to H_2 concentrations, but H_2 has a weak effect on para/meta-xylene ratios (Fig. 7). These data suggest that H_2 does not influence the strength of the acid sites, because an increase in acid strength would increase the surface residence times of adsorbed xylenes and thus the para/meta-xylene ratio. Therefore, H_2 appears to influence the density but not the strength of Brønsted acid sites. These data also show that H_2 does not increase hydrogen transfer rates, which would increase the rate of carbocation desorption. If this were the case, para/meta-xylene ratios would be closer to equilibrium at low H_2 pressures and decrease with increasing H_2 pressure. The rest of this study addresses the underlying mechanism for these unique H_2 effects on the density of acid sites, as well as the elementary steps required for *o*-xylene isomerization.

The mechanism of H_2 promotion was examined by measuring exchange rates between xylenes and D_2 after pretreatment in D_2 at reaction temperature. The rate of D-atom incorporation into xylenes (per W-atom) is 0.48×10^{-3} s^{-1} while the rate of isomerization via intramolecular methyl shifts per W-atom is $1.7 \times 10^{-3} s^{-1}$. The data in Fig. 8 also show that xylene adsorption–desorption steps are quasi-equilibrated, because all xylene isomers contain similar deuterium contents, as a result of frequent interactions between gas phase xylenes and Brønsted acid sites. The equivalent D-content in all xylenes suggests that D-atoms from D_2 in the gas phase are not required for carbocation desorption. If hydrogen transfer steps from D_2 to adsorbed xylenes were required for carbocation desorption, the deuterium content in products would be higher than in reactants. These data suggest instead that deuterium atoms are incorporated into xylenes during xylene activation (protonation) and desorption (deprotonation) steps on Brønsted acid sites containing O–D groups, and that it is those acid sites that contain the D atoms from the gas phase D_2.

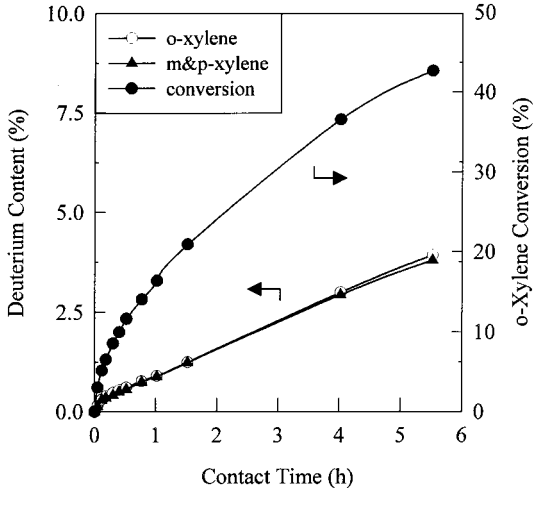

FIG. 8. Deuterium incorporation into xylene isomers as a function of contact time and *o*-xylene conversion (523 K, 114 kPa D_2, 0.66 kPa *o*-xylene, 15 wt% WO_x-ZrO_2; 8.4 WO_x/nm^2 surface density) (adapted from (7)).

These data lead us to suggest that the role of H_2 in increasing *o*-xylene isomerization rates (Fig. 7) reflects the formation of Brønsted acid sites via dissociation of H_2 on WO_x-ZrO_2 materials, as also suggested on Pt/SO_x-ZrO_2 (19) and Pt/WO_x-ZrO_2 (8). Quasi-equilibrated H_2 dissociation steps on two vacant sites would lead to H^* site densities and reaction rates proportional to $(H_2)^{0.5}$, but measured reaction rates are instead proportional to $(H_2)^{1.0}$ (Fig. 7). The involvement of two adjacent active sites in a H_2 dissociation step or in a catalytic turnover is not likely on WO_x-ZrO_2, because H_2 chemisorption uptakes show that the number of chemisorbed H atoms per W atom is very small (~0.06 H atoms/W atom at 523 K and 80 kPa H_2 (14)). Thus, the probability of neighboring sites is also very small. The observed first-order dependence would require either that H_2 dissociation be an irreversible step, or that H_2 dissociates with only one of the two H atoms used in the formation of Brønsted acid sites. H_2 dissociation steps cannot be irreversible because hydrogen is not consumed during xylene isomerization. We conclude, therefore, that only one acidic O–H is formed upon activation of a H_2 molecule. A possible mechanism for this process is shown in Scheme 4.

The isotopic exchange between D_2 and O–H groups suggests that H_2 dissociation occurs on WO_x-ZrO_2 materials at 523 K. More specifically, dissociation appears to occur on ZrO_2 surfaces not covered by WO_x species (14). The reversible dissociation of H_2 on ZrO_2 to form Zr–H and O–H groups has been reported previously (20, 21). Thus, we suggest that the reversible dissociation of H_2 on ZrO_2 leads to a catalytically inactive Zr–OH species and to mobile H atoms, which migrate to other Zr centers (21) or to WO_x domains. Active site formation then proceeds via the mechanism shown in Scheme 4, in which WO_x clusters stabilize $H^{\delta+}$ by electron transfer and charge delocalization across an extended WO_x framework. Similar processes form hydrogen bronzes (H_xWO_3) on WO_3 crystallites at room temperature, provided that H_2 dissociation sites are available (22). The charge in $H^{\delta+}$ species is compensated by a negative charge delocalized within WO_x domains to form $H^{\delta+}(WO_3)_n^{\delta-}$ Brønsted acid sites. UV-visible and Raman studies (23) confirm the formation of reduced W centers in WO_x–ZrO_2 materials when exposed to H_2 at 523 K. The formation of a Brønsted acid site and of a catalytically inactive hydroxyl from one H_2 molecule is consistent with the observed first-order dependence of *o*-xylene isomerization rates on H_2 concentration. The proposed mechanism for Brønsted acid site formation (Scheme 4) is also consistent with the low *o*-xylene isomerization rates observed on samples with predominantly monotungstate species (low

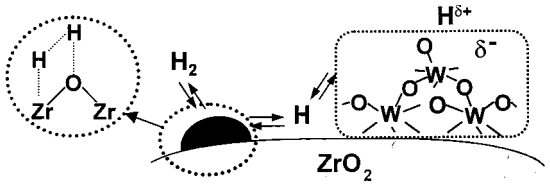

SCHEME 4. Formation of Brønsted acid sites by H_2.

WO_x surface density), which cannot delocalize the negative charge acquired during reduction over several W^{+6} atoms.

The formation of Brønsted acid sites by H_2 requires Lewis acid sites in the form of W^{+6} centers within neutral WO_x domains. These sites can be titrated by H adatoms to produce active Brønsted acid sites. Infrared studies of adsorbed ammonia and pyridine confirmed the presence of Lewis acid sites on these materials (24–26). In addition to their role as Brønsted acid site precursors, these Lewis acid sites may also catalyze *o*-xylene isomerization via radical cation chemistry (Scheme 5) (27) resulting in nonzero initial reaction rates even without H_2 in *o*-xylene reactants (Fig. 7).

The Effect of H_2 on Catalyst Deactivation Rates

H_2 also decreased catalyst deactivation rates, as shown by the semi-logarithmic plots of reaction rates vs time on stream shown in Fig. 9. Initial rates could be restored by treatment in air at 823 K, suggesting that deactivation is caused by carbon deposition. A first-order deactivation process, in which deactivation rates are proportional to the density of remaining active sites, leads to (28)

$$\frac{r}{r_0} = \exp(-\beta t). \qquad [2]$$

This equation predicts a semi-logarithmic relation between reaction rates and time on stream, a prediction confirmed by the data in Fig. 9. Equation [2] also allows the rigorous extrapolation of reaction rates to zero time on stream, which is required in order to obtain reliable values of *initial* isomerization turnover rates and to rigorously distinguish the effects of H_2 on reaction rates and on deactivation rates.

At a constant or low *o*-xylene conversion level, β (Eq. [2]) is also constant, because reactant and product concentrations vary slightly (or not at all) with time on stream. The dependence of deactivation rates on both *o*-xylene and

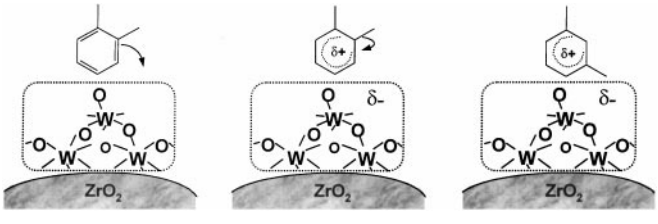

SCHEME 5. Proposed mechanism of *o*-xylene isomerization on Lewis acid sites.

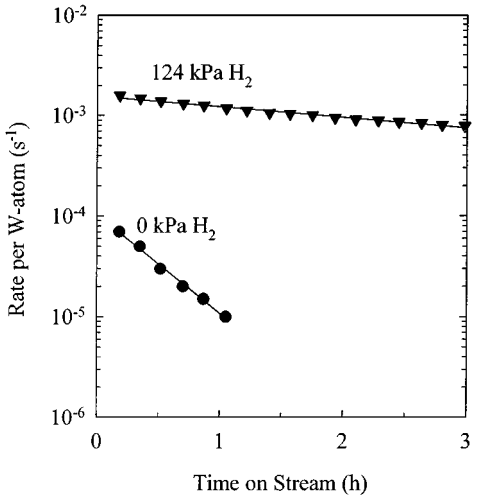

FIG. 9. Effect of H_2 on catalyst deactivation rates. Lines were obtained by linear least-squares fitting of the data (523 K, 0–124 kPa H_2, 0.66 kPa *o*-xylene, 15 wt% WO_x-ZrO_2; 8.4 WO_x/nm^2 surface density).

H_2 pressure was determined at low conversions (<5%). Figure 10 shows the effect of *o*-xylene concentration on the deactivation parameter β at a constant H_2 pressure (127 kPa). At high *o*-xylene concentrations, active sites become saturated with adsorbed xylene and deactivation rates do not depend on xylene concentration. The apparent Langmuir–Hinshelwood-type expression allows us to estimate deactivation rate parameters and the adsorption enthalpy and entropy (as obtained from the adsorption/desorption coefficient) for both deactivation and isomerization (Table 4). The data in Table 4 show that adsorption enthalpies and entropies for the two processes are equal within 95% confidence limits, suggesting that the denominators of both β and the isomerization rate expression

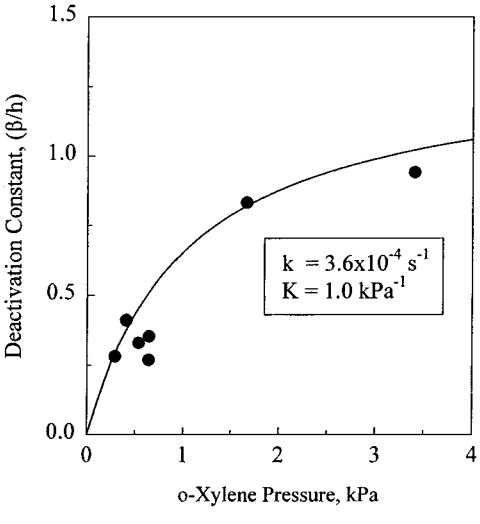

FIG. 10. Dependence of the deactivation constant (β) on *o*-xylene pressure (523 K, 127 kPa H_2, 0.2–3.5 kPa *o*-xylene, 15 wt% WO_x-ZrO_2; 8.4 WO_x/nm^2 surface density).

TABLE 4

Comparison of *o*-Xylene Isomerization and Deactivation Adsorption Parameters

	Reaction	Deactivation
K (at 523 K)	0.9 ± 0.1	1.0 ± 0.1
ΔH_{ads}, kcal/mol	-16.6 ± 2.1	-12.0 ± 5.6
ΔS_{ads}, cal/mol K	-31.7 ± 4.2	-22.7 ± 10.5

(Eq. [1]) are the same. This conclusion is relevant to the mechanistic model presented next.

The dependence of β on H_2 pressure (Fig. 11) and the deactivation rates shown in Fig. 9 show that deactivation pathways are inhibited by small amounts of H_2 (>9 kPa H_2). Higher H_2 concentrations influence deactivation rates only slightly. The complete removal of H_2, however, results in an increase in the deactivation rate by about a factor of 10 (Fig. 11). These data suggest that two pathways are responsible for the observed deactivation. Xylene dehydrogenation (via C–H bond activation and H-atom migration) proceeds in the absence of H_2 (Scheme 6; step f). This process is accompanied, at all H_2 pressures, by irreversible xylene adsorption on Lewis acid sites (as discussed below). Both processes lead to a decrease of the density of available active sites and of reaction rates with time on stream.

Hydrogen abstraction from *o*-xylene is consistent with the D_2/*o*-xylene isotopic exchange data. The slow rate of D-atom incorporation into xylenes may reflect the higher abundance of O–H groups on WO_x-ZrO_2, even though samples were treated in D_2 before reaction and D_2 was present during reaction. O–D groups formed during the initial D_2 treatment may be rapidly replaced by H atoms formed via reversible dehydrogenation of adsorbed xylenes.

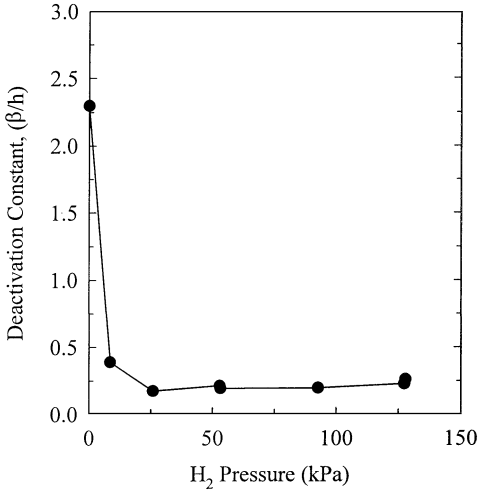

FIG. 11. Dependence of the deactivation constant (β) on H_2 pressure (523 K, 0–127 kPa H_2, 0.66 kPa *o*-xylene, 15 wt% WO_x-ZrO_2; 8.4 WO_x/nm^2 surface density).

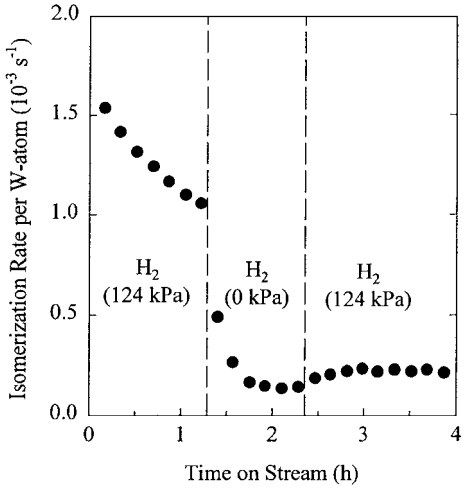

FIG. 12. Effect of mid-experiment removal of H_2 from the gas phase (523 K, 0–124 kPa H_2, 0.66 kPa *o*-xylene, 15 wt% WO_x-ZrO_2; 8.4 WO_x/nm^2 surface density).

In the absence of H_2, catalyst deactivation can occur by carbon deposition, and also by the desorption of H atoms that formed $H^{\delta+}(WO_3)_n^{\delta-}$ groups either during pretreatment or from C–H activation of *o*-xylene during reaction. The latter proceeds via the microscopic reverse of the dissociation, migration, and reduction processes that lead to the formation of these Brønsted acid sites when H_2 is present. In agreement with this, the effect of H_2 is reversible, since removal of H_2 during *o*-xylene isomerization results in a rapid decrease in catalytic activity (Fig. 12). The reintroduction of H_2 does not restore initial catalytic activity because irreversible deactivation events have occurred during *o*-xylene reactions in the absence of H_2. The removal of H_2 increases the density of Lewis sites, the adsorption of xylenes on these acid sites, and the desorption of hydrogen as H_2; as H_2 leaves the reactor, dehydrogenated xylene species remain irreversibly adsorbed on active sites.

The Effect of H_2 Pressure during Catalyst Pretreatment on Reaction Rates

A catalyst pretreatment in H_2 is required for high initial *o*-xylene isomerization rates on WO_x-ZrO_2 (Fig. 13). When the catalyst is treated in H_2 and the *o*-xylene reaction is also carried out in 127 kPa H_2, the initial isomerization rate is 1.7×10^{-3} s^{-1} (Table 1 and Fig. 13). If the catalyst is not treated in H_2 or if the xylene reaction is carried out without H_2, initial isomerization rates are about 10 times smaller (0.2×10^{-3} s^{-1}) (Table 1 and Fig. 13). If the catalyst is initially treated in He and H_2 is then introduced with the *o*-xylene reactants, isomerization rates increase to a maximum value of 0.9×10^{-3} s^{-1} during the first 0.5 h (Fig. 13). This increase in isomerization activity reflects the *in situ*

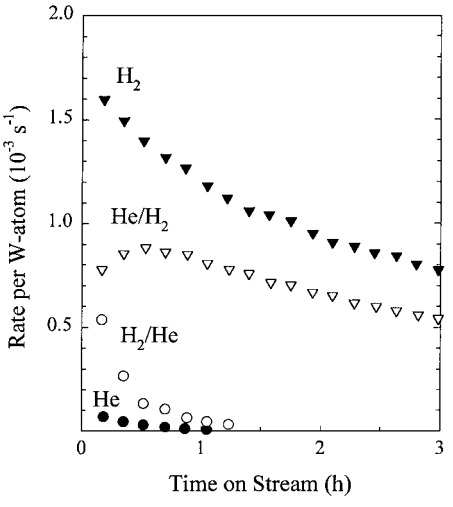

FIG. 13. Effect of catalyst pretreatment and reaction conditions on *o*-xylene isomerization activity. Data are labeled with *X*/*Y* or simply *Z*, where *X* represents the pretreatment atmosphere, *Y* represents the reaction atmosphere, and *Z* represents both pretreatment and reaction atmospheres. Thus samples treated in helium and operated in helium are labeled "He" and denoted by (●). Samples treated in H_2 and operated in helium are labeled "H_2/He" and denoted by (○). Samples treated in helium and operated in H_2 are labeled "He/H_2" and denoted by (▽). Samples treated and operated in H_2 are labeled "H_2" and are denoted by (▼) (523 K, 0–124 kPa H_2, 0.66 kPa *o*-xylene, 15 wt% WO_x-ZrO_2; 8.4 WO_x/nm^2 surface density).

formation of Brønsted acid sites when H_2 is present during *o*-xylene isomerization at 523 K by the mechanism described in Scheme 4. Isomerization rates never reach those measured on WO_x-ZrO_2 samples pretreated and operated in H_2 (1.7×10^{-3} s^{-1}) because irreversible deactivation of WO_x domains occurs during the initial stages of *o*-xylene isomerization before H_2 forms equilibrium surface densities of active $H^{\delta+}(WO_3)_n^{\delta-}$ species. When the catalyst is treated in H_2 and *o*-xylene reactions are then carried out without H_2, isomerization rates decrease rapidly (Fig. 13), consistent with the effect of H_2 removal shown in Fig. 12. These data confirm that active site formation in H_2 is reversible and that H_2 is required to form and maintain active sites required for xylene isomerization.

Modified Elementary Steps in o-Xylene Isomerization on WO_x-ZrO_2

In order to account for deactivation steps related to the process in Scheme 4, the catalytic sequence in Scheme 2 must include a contribution of Lewis acid sites to isomerization reactions and the loss of active sites by strongly adsorbed unsaturated species. The modified scheme (Scheme 6) includes the reversible formation of actives sites via mobile H atoms (H_M or H* in steps (a) and (b), *o*-xylene adsorption (step c), isomerization (step d), and desorption (step e) on Lewis acid sites, and deactivating events via *o*-xylene dehydrogenation (step f) and by irreversible adsorption of xylene (step g), in addition to the steady-state isomerization sequence in Scheme 2 (boxed equations).

The elementary steps leading to the isomerization of *o*-xylene on Brønsted acid sites (Scheme 2 and boxed equations in Scheme 6) can be assumed to remain at pseudo-steady-state, because the formation and loss of acid sites occur more slowly than isomerization steps, as shown by the long characteristic times in the rate transients in Figs. 12 and 13. Thus, the formation and destruction of acid sites varies only the concentration of Brønsted acid sites and not the position of the steady-state for xylene isomerization steps.

The active site (*) in Scheme 2 has been replaced with (H*), a species that can acquire a net positive charge at least in the activated complexes required for isomerization steps. The formation of these (H*) species occurs via dissociation of H_2 to form a Zr–OH group (H_I in step a) and a mobile H-atom (H_M in step a). These mobile H atoms then migrate to WO_x centers to form $H^{\delta+}(WO_3)_n^{\delta-}$ species (step b). In Scheme 6, (*) represents a Lewis acid site (W^{+6}), X* represents the concentration of xylenes adsorbed on Lewis acid sites, and X″* represents a deactivated catalyst site. In Scheme 6, two deactivation pathways (steps f and g) are included in order to account for the observed dependence of β (the deactivation rate constant in Eq. [2]) on both xylene and H_2 concentrations. The dehydrogenation of adsorbed *o*-xylene via C–H bond activation on a Lewis acid site (step f) is assumed to be quasi-equilibrated in the presence of H_2, but when H_2 is not present this step becomes irreversible because of the continuous loss of H_2 from the reactor and it leads to the net disappearance of $H^{\delta+}(WO_3)_n^{\delta-}$ species. In the presence of H_2, only step (g) leads to deactivation; without H_2, both (f) and (g) decrease the density of $H^{\delta+}(WO_3)_n^{\delta-}$ species. These proposed deactivation processes lead to the observed effects of H_2 on catalyst deactivation rates (Fig. 11).

a)	H_2	⇌	$H_M + H_I$	K_a
b)	H_M + *	⇌	H*	K_b
1)	X + H*	⇌	XH*	K_1
2)	XH*	→	X'H*	k_2
3)	X'H*	⇌	X' + H*	K_3
c)	X + *	⇌	X*	K_c
d)	X*	→	X'*	k_d
e)	X'*	⇌	X' + *	K_e
f)	X*	⇌	X"* + H	K_f
g)	X*	→	X"*	k_g

SCHEME 6. Modified mechanism accounting for promoting effects of H_2, Lewis acid-catalyzed isomerization, and catalyst deactivation. Boxed expressions reflect the previous isomerization reaction scheme (Scheme 2) in which * has been replaced with H* (a Brønsted acid active site).

The rate expression obtained for steady-state *o*-xylene isomerization on $H^{\delta+}(WO_3)_n^{\delta-}$ species (Eq. [1]) can be modified to account for H_2 effects by including the H^* formation pathways in Scheme 6. This effect was previously (and inadvertently) lumped into the number of catalyst sites, or (L) term, in Eq. [1]. The correct expression for (L) in Scheme 1, as derived from a site balance on steps a through g in Scheme 6, is

$$(L) = \frac{K_a K_b(H_2)[(L_0) - (X''^*)]}{1 + K_a K_b(H_2) + K_c(X)}, \quad [3]$$

where L_0 represents the maximum number of potential active sites. Substituting Eq. [3] into Eq. [1] leads to a rate expression for *o*-xylene isomerization on Brønsted acid sites:

$$r = \frac{k_2 K_1 K_a K_b(X)(H_2)[(L_0) - (X''^*)]}{[1 + K_1(X)][1 + K_a K_b(H_2) + K_c(X)]}. \quad [4]$$

Here, we have again neglected the contribution of the xylene product isomers (X'), because at low conversions (<5%), *o*-xylene is the predominant xylene isomer. Similarly, *o*-xylene isomerization rates on Lewis acid sites are given by

$$r = \frac{k_d K_c(X)[(L_0) - (X''^*)]}{1 + K_a K_b(H_2) + K_c(X)}. \quad [5]$$

Combining Eqs. [4] and [5] gives the total *o*-xylene isomerization rate

$$r = \underbrace{\left\{ \frac{k_2 K_1 K_a K_b(X)(H_2)[(L) - (X''^*)]}{[1 + K_1(X)][1 + K_a K_b(H_2) + K_c(X)]} \right\}}_{\text{(Brønsted acid sites)}} + \underbrace{\left\{ \frac{k_d K_c(X)[(L) - (X''^*)]}{1 + K_a K_b(H_2) + K_c(X)} \right\}}_{\text{(Lewis acid sites)}}. \quad [6]$$

The first term in Eq. [6] accounts for *o*-xylene isomerization on Brønsted acid sites. The second term reflects the rate of xylene isomerization on Lewis acid sites and it accounts for the nonzero reaction rates observed even in the absence of H_2 (Fig. 7). Equation [6] predicts that deactivation will occur as (X'') increases. The time dependence of X'' is given by a transient site balance

$$\frac{d(X''^*)}{dt} = k_g K_c(X)(^*) \quad [7]$$

in the presence of H_2 and

$$\frac{d(X''^*)}{dt} = k_g K_c(X)(^*) + k_f K_c(X)(^*) \quad [8]$$

when isomerization is carried out without H_2. Substituting the expression for $(^*)$ obtained from an overall site balance into Eqs. [7] and [8] and integrating gives

$$(L_0) - (X''^*) = (L_0)\exp(-\beta t), \quad [9]$$

where β is given by the expression

$$\beta = \frac{k_g K_c(X)}{1 + K_a K_b(H_2) + K_c(X)} \quad \text{(in } H_2\text{)} \quad [10]$$

$$\beta = \frac{k_g K_c(X) + k_f K_c(X)}{1 + K_a K_b(H_2) + K_c(X)} \quad \text{(in He)}. \quad [11]$$

Substituting Eq. [9] into Eq. [6] gives

$$r = \left[\frac{k_{\text{eff},1}(X)(H_2)}{[1 + K_1(X)]} + k_{\text{eff},2}(X) \right] \frac{(L_0)\exp(-\beta t)}{1 + K_a K_b(H_2) + K_c(X)}, \quad [12]$$

where

$$k_{\text{eff},1} = k_2 K_1 K_a K_b \quad [13]$$

$$k_{\text{eff},2} = k_d K_c. \quad [14]$$

For β to show the observed dependence on *o*-xylene concentration when H_2 is present (Eq. [10], Fig. 10) and no H_2 dependence as H_2 pressure increases (Fig. 11), the $K_a K_b(H_2)$ term, which represents the density of Brønsted acid sites, must be smaller than the other two denominator terms (1 and $K_c(X)$), which account for the density of Lewis acid sites and of xylene adsorbed on these acid sites, respectively. This conclusion is consistent with H_2 chemisorption measurements, which showed that the fraction of the surface containing Brønsted acid sites on these WO_x-ZrO_2 materials is very small (H atoms/W atom $\sim$ 0.06) (14). Also, if the denominator in the rate expression (Eq. [12]) and in the expression for β (Eqs. [10] and [11]) are indeed the same, as suggested by the numerical values of the reaction and deactivation adsorption parameters (Table 4), the $K_1(X)$ term in the denominator of Eq. [12] must be significantly less than unity (i.e., the density of Brønsted acid sites must be larger than the surface concentration of xylenes adsorbed on Brønsted acid sites). With these assumptions, Eq. [12] becomes

$$r = [k_{\text{eff},1}(X)(H_2) + k_{\text{eff},2}(X)] \frac{(L_0)\exp(-\beta t)}{1 + K_c(X)}. \quad [15]$$

Equation [15] is consistent with the first-order dependence of isomerization rates on H_2 pressure, with the observed Langmuir–Hinshelwood dependence on *o*-xylene concentration, and with the nonzero reaction rate observed in the absence of H_2. In addition, Eq. [7] shows that β has a Langmuir–Hinshelwood dependence on *o*-xylene pressure and it is independent of H_2 pressure as long as some H_2 is present in the reactant mixture. Finally, a comparison of Eqs. [10] and [11] shows that the absence of H_2 would lead to higher deactivation rates, as observed experimentally (Fig. 11). Thus, the proposed mechanism describing

reaction and deactivation during *o*-xylene isomerization on WO_x-ZrO_2 materials is entirely consistent with the kinetic and deactivation data reported in this study.

Using Eq. [15], expressions describing the previously measured kinetic parameters k_2 and K_1 in Eq. [1] can be derived.

$$k_2\,(\text{Eq. [1]}) = \frac{k_2 K_1 K_a K_b (H_2)}{K_c} \quad [16]$$

$$k_1\,(\text{Eq. [1]}) = K_c. \quad [17]$$

The measured effective rate constant for methyl shifts (k_2 in Eq. [1]) showed preexponential factors much lower than predicted for surface unimolecular isomerization steps. The reason is now apparent in light of Eq. [16]. The measured rate constant contains equilibrium constants for xylene adsorption/desorption steps on Brønsted acid sites (K_1), for xylene and H_2 adsorption/desorption steps on Lewis acid sites (K_c and K_a, respectively), and for H_2 dissociation (K_b). Thus the true expression for the preexponential factor reported in Table 2 is

$$A_{1,\text{effective}} = \frac{A \exp(\Delta S_1/R) \exp(\Delta S_a/R) \exp(\Delta S_b/R)(H_2)}{\exp(\Delta S_c/R)}. \quad [18]$$

This expression accounts for the discrepancy between the measured value of the preexponential factor and that predicted from transition state theory using the simplified steps of Scheme 6. The numerical values of these constants (K_1, K_a, and K_b) must be determined as a function of temperature in order to determine the true preexponential factor for the surface isomerization step (k_2).

CONCLUSIONS

A kinetic study of *o*-xylene isomerization established the role of H_2 in Brønsted acid site formation on metal-free WO_x-ZrO_2 catalysts at 523 K. The direct involvement of H_2 in catalytic turnovers was determined by D_2/*o*-C_8H_{10} isotopic exchange and the observed first-order dependence of isomerization rates on H_2 pressure. Independent H_2 chemisorption studies have shown a direct correlation between the amount of H_2 adsorbed by WO_x-ZrO_2 and *o*-xylene isomerization rates. This promotion of reaction rates by H_2 reflects the formation of Brønsted acid sites in H_2. Independent UV-visible adsorption and D_2-OH isotopic exchange studies suggest that active site formation proceeds via the reduction of WO_x domains by dissociated H_2 atoms and charge compensation by $H^{\delta+}$ species that serve as Brønsted acid sites. The addition of H_2 also decreases catalyst deactivation rates during *o*-xylene isomerization by maintaining the Brønsted acid site concentration and reversing xylene dehydrogenation steps that lead to coke formation. A kinetic model describing the isomerization of *o*-xylene in the presence and absence of H_2 was developed based on the results of *o*-$^{13}C_8H_{10}$/*o*-C_8H_{10} and D_2/*o*-C_8H_{10} isotopic exchange experiments and xylene and H_2 kinetic studies. This model is in good agreement with experimental observations.

APPENDIX: NOMENCLATURE

(X)	Gas phase concentration of *o*-xylene reactants
(X′)	Gas phase concentration of *m*- and *p*-xylene isomers
(H_2)	Hydrogen concentration
(H_M)	Concentration of mobile H-atoms
(H_I)	Concentration of immobile H-atoms
(*)	Lewis acid site concentration
(X*)	Concentration of xylene adsorbed on Lewis acid sites
(X′*)	Concentration of product xylene adsorbed on Lewis acid sites
(H*)	Brønsted acid site concentration
(XH*)	Concentration of xylene adsorbed on Brønsted acid sites
(X′H*)	Concentration of product xylene adsorbed on Brønsted acid sites
(X″*)	Concentration of sites deactivated by irreversibly adsorbed xylenes
(L)	Total site concentration in Scheme 2
(L_0)	True total site concentration
K_a	Equilibrium constant for H_2 dissociation
K_b	Equilibrium constant for Brønsted acid site formation
K_1	Equilibrium constant for *o*-xylene adsorption/desorption on Brønsted acid sites
k_2	Rate constant for the methyl shift step on Brønsted acid sites
K_3	Equilibrium constant for *m*- and *p*-xylene adsorption/desorption on Brønsted acid sites
K_c	Equilibrium constant for *o*-xylene adsorption/desorption on Lewis acid sites
k_d	Rate constant for the methyl shift step on Lewis acid sites
K_e	Equilibrium constant for *m*- and *p*-xylene adsorption/desorption on Lewis acid sites
K_f	Equilibrium constant for *o*-xylene hydrogenation/dehydrogenation
k_g	Rate constant for irreversible *o*-xylene adsorption on Lewis acid sites
β	Deactivation constant

ACKNOWLEDGMENTS

This work was funded by the National Science Foundation (CTS-9510575) under the technical guidance of Dr. Raul Miranda. We are grateful to Dr. Stuart L. Soled (Exxon Mobil Research and Engineering Co.) for useful technical discussions and comments.

REFERENCES

1. Hino, M., and Arata, K., *J. Chem. Soc. Chem. Comm.* 1259 (1987).
2. Chang, C. D., Santiesteban, J. G., and Stern, D. L., 1993, U.S. Patent # 5,345,026.
3. Larsen, G., and Petkovic, L., *Appl. Catal. A* **148**, 155 (1996).
4. Santiesteban, J. G., Vartuli, J. C., Han, S., Bastian, R. D., and Chang, C. D., *J. Catal.* **168**, 431 (1997).
5. Petkovic, L. M., Bielenberg, J. R., and Larsen, G., *J. Catal.* **178**, 533 (1998).
6. Barton, D. G., Soled, S. L., and Iglesia, E., *Topics in Catal.* **6**, 87 (1998).
7. Barton, D. G., Soled, S. L., Meitzner, G. D., Fuentes, G. A., and Iglesia, E., *J. Catal.* **181**, 57 (1999).
8. Iglesia, E., Barton, D. G., Soled, S. L., Miseo, S., Baumgartner, J. E., Gates, W. E., Fuentes, G. A., and Meitzner, G. D., *Stud. Surf. Sci. Catal.* **101**, 533 (1996).
9. Price, G. L., and Iglesia, E., *Ind. Eng. Chem.* **28**, 839 (1989).
10. Iglesia, E., Baumgartner, J. E., Price, G. L., Rose, K. D., and Robbins, J. L., *J. Catal.* **125**, 95 (1990).
11. Ryan, T. P., "Handbook of Statistical Methods for Engineers and Scientists" (H. M. Wadsworth, Ed.), McGraw–Hill, New York, 1989.
12. Morin, S., Ayrault, P., Mouahid, S. E., Gnep, N. S., and Guisnet, M., *Appl. Catal. A* **159**, 317 (1997).
13. Pitzer, K. S., and Scott, D. W., *J. Am. Chem. Soc.* **65**, 803 (1943).
14. Baertsch, C. D., Soled, S. L., and Iglesia, E., unpublished results, 1999.
15. Li, Y.-g., Chang, X., and Zeng, Z., *Ind. Eng. Chem. Res.* **31**, 187 (1992).
16. Morin, S., Gnep, N. S., and Guisnet, M., *J. Catal.* **159**, 296 (1996).
17. Ma, Y. H., and Savage, L. A., *AIChE J.* **33**(8), 1233 (1987).
18. Boudart, M., "Physical and Chemical Engineering Series" (N. R. Amundson, Ed.), Prentice Hall, New York, 1968.
19. Hattori, H., and Shishido, T., *Catal. Surveys Japan* **1**, 205 (1997).
20. Onishi, T., Abe, H., Maruya, K.-i., and Domen, K., *J. Chem. Soc. Chem. Comm.* **617** (1985).
21. Jacob, K. H., Knozinger, E., and Benfer, S., *J. Chem. Soc. Faraday Trans.* **90**(19), 2969 (1994).
22. Benson, J. E., Kohn, H. W., and Boudart, M., *J. Catal.* **5**, 307 (1966).
23. Barton, D. G., Shtein, M., Wilson, R. D., Soled, S. L., and Iglesia, E., *J. Phys. Chem. B* **103**, 630 (1999).
24. Larsen, G., Raghavan, S., Marquez, M., and Lotero, E., *Catal. Lett.* **37**, 57 (1996).
25. Scheithauer, M., Cheung, T.-K., Jentoft, R. E., Grasseli, R. K., Gates, B. C., and Knozinger, H., *J. Catal.* **180**, 1 (1998).
26. Baertsch, C. D., Barton, D. G., Wilson, R. D., Soled, S. L., and Iglesia, E., *Stud. Surf. Sci. Catal.* **130**, 3225 (2000).
27. Franklin, J. L., and Nicholsen, D. E., *J. Phys. Chem.* **60**, 59 (1956).
28. Butt, J. B., and Peterson, E., "Activation, Deactivation, and Poisoning of Catalysts." Academic Press, San Diego, 1988.